

Order from structural disorder in XY pyrochlore antiferromagnet $\text{Er}_2\text{Ti}_2\text{O}_7$

V. S. Maryasin¹ and M. E. Zhitomirsky²

¹*University Grenoble-Alps and INAC-SPSMS, F-38000 Grenoble, France*

²*Service de Physique Statistique, Magnétisme et Supraconductivité,
UMR-E9001 CEA-INAC/UJF, 17 rue des Martyrs, 38054 Grenoble Cedex 9, France*

(Dated: June 27, 2021)

Effect of structural disorder is investigated for an XY pyrochlore antiferromagnet with continuous degeneracy of classical ground states. Two types of disorder, vacancies and weakly fluctuating exchange bonds, lift degeneracy selecting the same subset of classical ground states. Analytic and numerical results demonstrate that such an “order by structural disorder” mechanism competes with the effect of thermal and quantum fluctuations. Our theory predicts that a small amount of nonmagnetic impurities in $\text{Er}_2\text{Ti}_2\text{O}_7$ will stabilize the coplanar ψ_3 ($m_{x^2-y^2}$) magnetic structure as opposed to the ψ_2 ($m_{3z^2-r^2}$) state found in pure material.

PACS numbers: 75.10.-b, 75.50.Ee, 75.40.Mg

I. INTRODUCTION

Geometrically frustrated magnets with competing exchange interactions often display continuous, symmetry unrelated degeneracy of classical ground states. Such an ‘accidental’ degeneracy may be lifted by weak additional interactions. Those are always present in real materials but can significantly vary even between similar compounds. Therefore, a lot of studies on frustrated magnets have been devoted to understanding the universal degeneracy-lifting mechanism produced by thermal and quantum fluctuations. The corresponding concept named “order by disorder” was pioneered by Villain *et al.* [1] and Shender [2] and, in a nutshell, relates the ground-state selection to softer excitation spectrum for certain degenerate states. Being investigated for numerous spin models, the order by disorder mechanism finds so far only a few realizations in magnetic materials. Perhaps the clearest examples of the order by disorder selection are provided by the 1/3-magnetization plateau in triangular-lattice antiferromagnets [3–6] and by a zero-field noncoplanar spin structure of the XY pyrochlore antiferromagnet $\text{Er}_2\text{Ti}_2\text{O}_7$ [7, 8].

Weak lattice disorder, if present in a magnetic solid, changes locally parameters of the spin Hamiltonian and can also affect the ground state selection [9–12]. For a few studied models, the structural disorder tends to select classical ground-states in precisely the opposite manner compared to the thermal and quantum effects. These include an orthogonal magnetic structure for the J_1 – J_2 square lattice antiferromagnet [9, 11] and a conical state for the Heisenberg triangular-lattice antiferromagnet in an external field [12]. In our previous work, such a difference was explained by opposite signs of effective biquadratic interactions generated by two types of the order from disorder: thermal and quantum fluctuations yield a negative biquadratic exchange [13, 14], whereas bond and site disorder produce a positive biquadratic term [12]. Note, that in a rather different context a positive biquadratic coupling in ferromagnetic multilayers

was attributed to interface roughness [15].

The known examples bring up a problem of further generalization of the above principle. Specifically, for some highly symmetric frustrated spin models, an effective interaction that is able to lift the classical degeneracy appears only beyond the fourth-order terms in the Landau energy functional. Then, a biquadratic coupling of either sign leaves degeneracy intact raising again the question about the outcome of the order from structural disorder selection.

As a matter of fact, such a highly symmetric frustrated spin model is realized in the anisotropic XY pyrochlore $\text{Er}_2\text{Ti}_2\text{O}_7$ [16–22]. This pyrochlore material orders at $T_N \simeq 1.2$ K into a noncoplanar $k = 0$ antiferromagnetic structure called the ψ_2 state [16, 17]. To emphasize its symmetry properties we shall denote this state as $m_{3z^2-r^2}$ in the following. At the mean-field level, there is no energy difference between the $m_{3z^2-r^2}$ state and the coplanar $m_{x^2-y^2}$ (ψ_3) state, see Fig. 1. The two states form a basis of the E irreducible representation of the tetrahedral point group and can be continuously turned into each other by simultaneous rotation of four sublattices. Such degeneracy persists even with an extra biquadratic exchange, but the harmonic spin-wave calculations indicate that fluctuations choose the noncoplanar $m_{3z^2-r^2}$ state [7, 8, 23–26]. Therefore, it is instructive to study the role of structural disorder, in particular, nonmagnetic vacancies, on degeneracy lifting for the XY pyrochlore antiferromagnet. This is even more so in view of well established experimental possibility to systematically substitute nonmagnetic ions in pyrochlore materials [27, 28].

In the present work we study theoretically the effect of structural disorder on the classical XY pyrochlore antiferromagnet. Similar to other frustrated models, structural disorder favors in this case a different subset of classical ground states compared to those selected by quantum and thermal fluctuations. Specifically, we predict that nonmagnetic impurities substituted into $\text{Er}_2\text{Ti}_2\text{O}_7$ will stabilize the coplanar $m_{x^2-y^2}$ antiferromagnetic state. The paper is organized as fol-

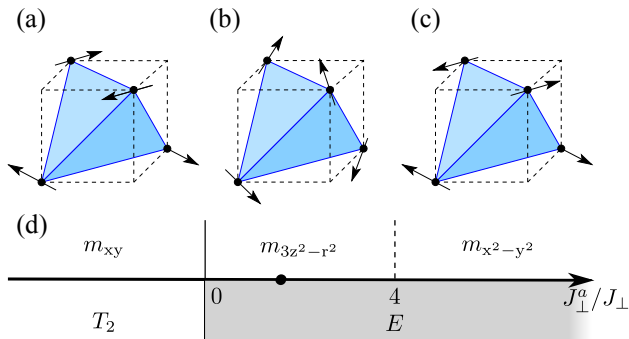


FIG. 1. (Color online) Ordered magnetic structures of the XY pyrochlore antiferromagnet: (a) the coplanar Palmer-Chalker state m_{xy} , (b) the noncoplanar state $m_{3z^2-r^2}$, and (c) the coplanar state $m_{x^2-y^2}$. (d) Schematic phase diagram of the model (1) showing the lowest-energy magnetic structures depending on the ratio J_{\perp}^a/J_{\perp} . Circle marks the value of J_{\perp}^a/J_{\perp} in $\text{Er}_2\text{Ti}_2\text{O}_7$.

lows. Section II describes the spin model appropriate for anisotropic XY pyrochlores. In Sec. III we develop an analytical approach to the problem of the ground state selection in the framework of the real-space perturbation theory. Section IV contains our main analytic result: corrections to the classical ground state energy produced by weak bond and site disorder. Numerical results in support of the analytic analysis include the ground-state energy minimization and Monte Carlo simulations and are described in Sec. V. In Sec. VI we discuss competition between state selection produced by quantum fluctuations and the structural disorder in view of possible realization in $\text{Er}_2\text{Ti}_2\text{O}_7$. Finally, Sec. VII contains conclusions and gives further outlook.

II. SPIN MODEL

Low-temperature magnetic properties of $\text{Er}_2\text{Ti}_2\text{O}_7$ and a number of other insulating pyrochlore materials are well approximated by an effective pseudo-spin-1/2 model for interacting Kramers doublets produced by strong crystal-field splitting. In the case of $\text{Er}_2\text{Ti}_2\text{O}_7$, the crystalline electric field determines the predominantly planar character of the lowest-energy Kramers doublets [16]. Correspondingly, the effective spin-1/2 Hamiltonian features the anisotropic XY interactions: [7]

$$\hat{\mathcal{H}} = \sum_{\langle ij \rangle} [J_{\perp} \mathbf{S}_i^{\perp} \cdot \mathbf{S}_j^{\perp} + J_{\perp}^a (\mathbf{S}_i^{\perp} \cdot \hat{\mathbf{r}}_{ij})(\mathbf{S}_j^{\perp} \cdot \hat{\mathbf{r}}_{ij})]. \quad (1)$$

Here $\hat{\mathbf{r}}_{ij} = (\mathbf{r}_i - \mathbf{r}_j)/|\mathbf{r}_i - \mathbf{r}_j|$ is a unit vector in the bond direction and spin components are taken with respect to the local axes such that the z_i direction coincides with the [111] axis and \mathbf{S}_i^{\perp} refers to the projection onto the orthogonal plane. We are interested in the case of antiferromagnetic exchange interactions $J_{\perp}, J_{\perp}^a > 0$ relevant to $\text{Er}_2\text{Ti}_2\text{O}_7$ and assume an arbitrary value of spin S

in order to separate classical and quantum effects in the framework of the semiclassical $1/S$ expansion. Further details on geometry of a pyrochlore lattice and different forms of the spin Hamiltonian (1) are provided in Appendix A.

We begin with description of the classical ground states of the spin model (1). Depending on the sign of J_{\perp}^a , magnetically ordered states belong to one of the two different classes, which transform according to E (Γ_5) or T_2 (Γ_7) irreducible representations of the tetrahedral point group. Figure 1(d) shows a classical ground state phase diagram of the model (1). For negative J_{\perp}^a the anisotropic exchange has the same effect as the long-range dipolar interactions. It selects the Palmer-Chalker states [29], represented by the m_{xy} state in Fig. 1(a). Their classical energy is $E_{T_2} = -S^2(J_{\perp} - \frac{1}{2}J_{\perp}^a)$. For $J_{\perp}^a > 0$ the ground state belongs to a two component E representation with the energy $E_E = -S^2(J_{\perp} + \frac{1}{2}J_{\perp}^a)$. Its basis is formed by the noncoplanar state $m_{3z^2-r^2}$ (ψ_2) and the coplanar $m_{x^2-y^2}$ (ψ_3) state. These are shown in Figs. 1(b) and 1(c), respectively. The value $J_{\perp}^a = 0$ is a highly degenerate point, where many states with different ordering wavevectors have the same classical energy [23].

Focusing on $J_{\perp}^a > 0$, we specify the local $\hat{\mathbf{x}}_i$ and $\hat{\mathbf{y}}_i$ axes on each site along the two E -states, see Appendix A, and parameterize the whole manifold of degenerate classical ground states with an angle φ

$$\mathbf{S}_i = \hat{\mathbf{x}}_i \cos \varphi + \hat{\mathbf{y}}_i \sin \varphi. \quad (2)$$

Values $\varphi = \pi k/3$ and $\varphi = \pi(k + \frac{1}{2})/3$ correspond to different $m_{3z^2-r^2}$ and $m_{x^2-y^2}$ states, respectively.

According to the group theory $m_{3z^2-r^2}$ and $m_{x^2-y^2}$ states remain strictly degenerate for a general case of the bilinear spin Hamiltonian involving further anisotropic terms or couplings to distant neighbors. An effective bi-quadratic exchange $(\mathbf{S}_i \cdot \mathbf{S}_j)^2$, does not lift this degeneracy either. The degeneracy may be lifted only by interactions of the sixth order in spin components, which are usually small in real materials. Hence, the spin model (1) provides an interesting example of the order from disorder selection. For $0 < J_{\perp}^a/J_{\perp} < 4$, thermal and quantum fluctuations favor the noncoplanar ground states of the type $m_{3z^2-r^2}$, including the point $J_{\perp}^a/J_{\perp} \sim 1.5$ corresponding to $\text{Er}_2\text{Ti}_2\text{O}_7$ [7, 8, 26]. For $J_{\perp}^a/J_{\perp} > 4$, the selection takes a different route and fluctuations stabilize the $m_{x^2-y^2}$ states [24]. The corresponding transition at $J_{\perp}^a = 4J_{\perp}$ is indicated by a dashed line in Fig. 1(d). In the next section we show that quantum and thermal corrections to the classical energy generate $E_{\text{eff}} \sim (J_{\perp}^a - 4J_{\perp}) \cos 6\varphi$ explaining the above transition.

III. REAL-SPACE PERTURBATION THEORY

The aim of this section is to present a simple analytic derivation of the previously obtained results [7, 8, 23, 24] on degeneracy lifting by thermal and quantum

fluctuations in the anisotropic XY pyrochlore. Instead of calculating excitation spectra around a few selected states, we use the real-space perturbation theory [12–14, 30, 31], which avoids numerical diagonalization and integrations procedures and treats all possible ground-state spin configurations on equal footing. Basically, the real-space expansion is a perturbative treatment of transverse spin fluctuations neglected in the mean-field approximation and, as such, is a variant of the $1/z$ expansion with z being a number of nearest neighbors (see Sec. III C).

A. General formalism

The real-space perturbation expansion starts with (i) rewriting the Hamiltonian in the local frame around an arbitrary ground-state spin configuration and (ii) separating all terms, which depend on deviation of only one spin. This on-site part is subsequently regarded as a non-interacting Hamiltonian $\hat{\mathcal{H}}_0$ with trivially calculated excited states. All other terms describe interactions of spin fluctuations on adjacent sites and are treated as a perturbation \hat{V} . Standard thermodynamic or quantum perturbation theories are used to calculate the effect of \hat{V} . The obtained correction terms generate effective spin-spin interactions beyond the original spin Hamiltonian and produce the order by disorder effect. For both quantum and thermal fluctuations, the second-order expansion generates effective biquadratic exchange terms [12–14]. Here, we need to go to the next third order to obtain effective degeneracy-lifting interactions in the case of $\text{Er}_2\text{Ti}_2\text{O}_7$.

To proceed with calculations for the anisotropic XY pyrochlore (1) we shall use an alternative form of the spin Hamiltonian

$$\hat{\mathcal{H}} = \sum_{\langle ij \rangle} [-J_{\pm}(S_i^+ S_j^- + S_i^- S_j^+) + J_{\pm\pm}(e^{i\gamma_{ij}} S_i^+ S_j^+ + e^{-i\gamma_{ij}} S_i^- S_j^-)], \quad (3)$$

where spin components are assigned for a specific choice of coordinate axes in the local xy planes, see Appendix A for definition of axes, bond dependent phases γ_{ij} and further details. In particular, the new exchange parameters are related to the original constants via

$$J_{\pm} = \frac{1}{12}(2J_{\perp} + J_{\perp}^a), \quad J_{\pm\pm} = \frac{1}{12}(4J_{\perp} - J_{\perp}^a). \quad (4)$$

These new interaction parameters coincide with those used by Savary *et al.* [8], though our spin Hamiltonian is written somewhat differently.

Next we transform to the sublattice basis such that the local z -axis becomes parallel to the spin direction (2) and the local x -axis lies in the respective easy plane. Spin components in the new coordinate frame are denoted by S^{α} . Then, the spin Hamiltonian takes the form

$$\hat{\mathcal{H}} = \sum_{\langle ij \rangle} [h_{ij} S_i^z S_j^z - M_{ij} S_i^x S_j^x - K_{ij} (S_i^x S_j^z + S_i^z S_j^x)], \quad (5)$$

where h_{ij} , M_{ij} , and K_{ij} are bond-dependent constants

$$\begin{aligned} h_{ij} &= -2J_{\pm} + 2J_{\pm\pm} \cos(2\varphi + \gamma_{ij}), \\ K_{ij} &= 2J_{\pm\pm} \sin(2\varphi + \gamma_{ij}), \\ M_{ij} &= 2J_{\pm} + 2J_{\pm\pm} \cos(2\varphi + \gamma_{ij}). \end{aligned} \quad (6)$$

They explicitly depend on angle φ , which parameterizes the classical ground states. Finally, we extract the on-site part and rewrite (5) as $\hat{\mathcal{H}} = \hat{\mathcal{H}}_0 + \hat{V}_1 + \hat{V}_2 + \hat{V}_3$, where

$$\begin{aligned} \hat{\mathcal{H}}_0 &= h \sum_i (S - S_i^z), \quad \hat{V}_1 = - \sum_{\langle ij \rangle} K_{ij} (S_i^x S_j^z + S_i^z S_j^x), \\ \hat{V}_2 &= - \sum_{\langle ij \rangle} M_{ij} S_i^x S_j^x, \quad \hat{V}_3 = \sum_{\langle ij \rangle} h_{ij} (S - S_i^z)(S - S_j^z). \end{aligned} \quad (7)$$

The constant $h = \sum_j h_{ij} = 12J_{\pm}S$ is an amplitude of a local magnetic field, which is the same on every site. In the above expression we also omitted a constant term corresponding to the classical energy. In the two following subsections we calculate the relevant energy corrections generated by thermal and quantum fluctuations.

B. Thermal Order by disorder

Here we consider a model of purely classical spins of unit length $|\mathbf{S}_i| = 1$. At low temperatures, spins fluctuate about their equilibrium directions by small S^x and S^y corresponding to deviations within the local easy plane and out of it, respectively. The local fluctuations are governed by

$$\hat{\mathcal{H}}_0 = \frac{h}{2} \sum_i (S_i^{x2} + S_i^{y2}). \quad (8)$$

The linear in S^x terms included in \hat{V}_1 vanish for the lowest-energy state. Thus, both \hat{V}_1 and \hat{V}_3 describe non-linear effects and produce higher-order contributions in T , which will be neglected in the following.

We now proceed with the classical thermodynamic perturbation theory to determine the free-energy correction generated by \hat{V}_2 . The calculation is rather straightforward [14] and we present only the final result. The second-order contribution $\Delta F^{(2)} = -\langle \hat{V}_2^2 \rangle / 2T$ is the same for all classical ground states (2). The leading state-dependent correction appears in the third order:

$$\Delta F^{(3)} = \frac{\langle \hat{V}_2^3 \rangle_0}{3T^2} = -\frac{2T}{(12J_{\pm})^3} \sum_{\Delta} M_{ij} M_{jk} M_{ki}, \quad (9)$$

where $\langle \dots \rangle_0$ denotes thermodynamic averaging with respect to $\hat{\mathcal{H}}_0$. Summation in (9) is performed over all triangular plaquettes of a pyrochlore lattice and $i, j, k \in \Delta$. Substituting M_{ij} from (6) we obtain

$$\Delta F^{(3)} \simeq -\frac{TJ_{\pm\pm}^3 N}{216J_{\pm}^3} \cos 6\varphi. \quad (10)$$

where N is the number of sites. Here and everywhere below \simeq sign means that ground state independent constant term has been omitted. The correction $\Delta F^{(3)}$ is linear in T reflecting the fact that it is produced by the harmonic fluctuations. It also has the six-fold symmetry in agreement with the Z_6 symmetry breaking in the $m_{3z^2-r^2}$ magnetic structure [26]. The respective term changes sign with $J_{\pm\pm}$, i.e., for $J_{\perp}^a/J_{\perp} = 4$, in total agreement with the phase diagram sketched in Fig. 1(d) and with the previous findings [24]. For the ratio of parameters $J_{\perp}^a/J_{\perp} \sim 1.5$ appropriate for $\text{Er}_2\text{Ti}_2\text{O}_3$, $J_{\pm\pm}$ is positive and thermal fluctuations select $\varphi = 0, \pi/3, \dots$ corresponding to the noncoplanar $m_{3z^2-r^2}$ spin configuration.

C. Quantum order by disorder

We now set $T = 0$ and use the Rayleigh-Schrödinger perturbation theory to calculate quantum corrections to the classical ground-state energy. For that we treat \mathbf{S}^{α} as spin operators obeying the standard commutation relations. Again we focus on the effect of \hat{V}_2 , which is more conveniently written in terms of spin raising and lowering operators

$$\hat{V}_2 = -\frac{1}{4} \sum_{\langle ij \rangle} M_{ij} (\mathbf{S}_i^+ + \mathbf{S}_i^-) (\mathbf{S}_j^+ + \mathbf{S}_j^-). \quad (11)$$

The ground state $|0\rangle$ of the noninteracting Hamiltonian $\hat{\mathcal{H}}_0$ coincides with a chosen classical ground state and corresponds to a ‘fully-saturated’ state in the rotated basis: $\mathbf{S}_i^+|0\rangle = 0$. The latter property yields $\langle 0|\hat{V}|0\rangle = 0$ and determines that every term in the perturbation series starts and ends with creation and annihilation of a pair of spin flips. For instance, the third-order correction is given by

$$\Delta E^{(3)} = \sum_{n,m} \frac{\langle 0|\hat{V}|n\rangle \langle n|\hat{V}|m\rangle \langle m|\hat{V}|0\rangle}{(E_0 - E_n)(E_0 - E_m)}, \quad (12)$$

where $|n\rangle$ and $|m\rangle$ are excited states of $\hat{\mathcal{H}}_0$ with $E_{n,m} = E_0 + 2h$. Since $h = O(z)$ and $\hat{V} = O(1)$, each extra order of the real-space expansion contributes a factor $1/z$ to the corresponding energy correction.

Detailed analysis of all second- and third-order terms in the real space perturbation expansion is presented in Appendix B. In particular, $\Delta E^{(2)}$ yields an energy shift which is independent of φ . Selection between different ground states is determined by the third-order excitation process described by the diagram

$$|000\rangle \xrightarrow{S_i^- S_j^-} |110\rangle \xrightarrow{S_j^+ S_k^-} |101\rangle \xrightarrow{S_k^+ S_i^+} |000\rangle \quad (13)$$

with three sites i, j, k belonging to the same triangular plaquette. The corresponding energy correction is given

by a plaquette sum

$$\Delta E^{(3)} = -6 \sum_{\Delta} \frac{S^3 M_{ij} M_{jk} M_{ki}}{8 (24J_{\pm}S)^2}. \quad (14)$$

Performing lattice summation and dropping an unimportant constant we obtain

$$\Delta E^{(3)} \simeq -\frac{J_{\pm\pm}^3 NS}{192J_{\pm}^2} \cos 6\varphi. \quad (15)$$

The quantum correction scales as $\Delta E^{(3)} = O(JS)$ and, thus, represents a harmonic spin-wave contribution. The full harmonic spin-wave calculation is, of course, not restricted to triangular plaquettes and includes graphs of all possible lengths [7]. However, for small $J_{\pm\pm}/J_{\pm}$ or $J_{\perp}^a \gtrsim 1$ its angular dependence as well as the corresponding prefactor are very closely reproduced by (15).

The third-order real-space correction contains also contribution $O(J)$, which goes beyond the harmonic spin-wave theory. It exhibits the same functional form as Eq. (15) but has the opposite sign and, therefore, partially compensates the energy difference between $m_{3z^2-r^2}$ and $m_{x^2-y^2}$ states. Overall, for $S = 1/2$ the amplitude of the sixfold harmonics (15) is reduced by 40% due to interaction effects, see Appendix C for further details.

IV. ORDER BY STRUCTURAL DISORDER

Structural disorder modifies locally exchange interactions and destroys perfect magnetic frustration at the microscopic level. As a result, magnetic moments tilt from the equilibrium bulk structure producing spin textures [32–34] and net uncompensated moments [34–36]. The idea of uncompensated moments and related local magnetic fields was also used by Henley in his explanation of vacancy-induced degeneracy lifting in the J_1 – J_2 square-lattice antiferromagnet [9]. Though simple and quite appealing, this approach cannot be applied to a general problem of ‘order by structural disorder’ in non-collinear frustrated magnets. Indeed, local fields from vacancies on different magnetic sublattices average to zero in a macroscopic sample producing no selection.

Building on the previous works [15, 10], we have recently shown that bond and site disorder generate positive biquadratic exchange [12]. Such an effective interaction is obtained by integrating out static fluctuations in a spin texture and due to its sign favors the *least* collinear spin configurations in degenerate frustrated magnets. Examples include an orthogonal state in the J_1 – J_2 square-lattice antiferromagnet [9, 11] and a conical state in the Heisenberg triangular antiferromagnet in an external magnetic field [12]. Here we extend our treatment of quenched disorder to the anisotropic XY pyrochlore (1). This requires calculation of the effective Hamiltonian beyond the leading biquadratic contribution. Also, note that the effect of structural disorder

on the equilibrium magnetic structure is essentially classical. Therefore, we assume throughout this section that spins are three-component classical vectors with $|\mathbf{S}_i| = 1$.

A. Nonmagnetic impurities

A single vacancy induces a strong local perturbation of the magnetic structure in noncollinear antiferromagnets [34]. To obtain qualitative insights within analytic treatment of the impurity problem we use a toy model of weak site disorder [10]. Specifically, we let some fraction n_{imp} of classical spins to be shorter by a small amount $\epsilon \ll 1$. These impurities are distributed randomly over the lattice and we assign a parameter $p_i = 1$ to every impurity spin and $p_i = 0$ otherwise: $\sum_i p_i = N_{\text{imp}}$. In the spin Hamiltonian impurities are included by substitution $\mathbf{S}_i \rightarrow \mathbf{S}_i(1 - \epsilon p_i)$ and in the leading order in ϵ we have for pairwise spin-spin interactions:

$$S_i^\alpha S_j^\beta \approx S_i^\alpha S_j^\beta [1 - \epsilon(p_i + p_j)]. \quad (16)$$

We perform the same decomposition of the spin Hamiltonian as described in Sec. III. The main difference with the preceding section is that linear in spin deviations part of \hat{V}_1 does not vanish:

$$\hat{V}_1' = \sum_{\langle ij \rangle} K_{ij} \epsilon (p_i + p_j) (\mathbf{S}_i^x + \mathbf{S}_j^x), \quad (17)$$

describing the fact that adjacent to impurity spins tilt from their equilibrium orientations in the bulk. Minimization of the quadratic form $\hat{H}_0 + \hat{V}_1$ over \mathbf{S}_i^x yields

$$\mathbf{S}_i^x = \frac{\epsilon}{12J_\pm} \sum_{j=1}^6 K_{ij} p_j, \quad (18)$$

where the sum runs over six nearest neighbors of the site i . Here, we neglected deviations of spins beyond the first-neighbor shell around an impurity in the spirit of the real-space perturbation expansion. Substitution of the new minimum condition into $\hat{\mathcal{H}}$ produces an energy correction. The leading term is obtained from $\hat{H}_0 + \hat{V}_1$ and gives an effective biquadratic exchange [12]. As before, this energy correction is independent of angle φ . Going to the next order we substitute (18) into \hat{V}_2

$$\Delta E_2 = -\frac{\epsilon^2}{(12J_\pm)^2} \sum_{\langle ij \rangle} M_{ij} \sum_{l,m=1}^6 K_{il} K_{jm} p_l p_m. \quad (19)$$

Keeping only terms that are linear in n_{imp} we can rewrite Eq. (19) as

$$\Delta E_2 = -\frac{\epsilon^2 n_{\text{imp}}}{(12J_\pm)^2} \sum_{\langle ij \rangle} \sum_{l=1}^2 M_{ij} K_{il} K_{jl}, \quad (20)$$

where the last summation is over two sites sharing the same tetrahedron with i and j . Finally, substituting expressions for bond-dependent parameters M_{ij} and K_{ij}

from (6) we obtain

$$\Delta E_2 \simeq \frac{J_{\pm\pm}^3 \epsilon^2 N_{\text{imp}}}{12J_\pm^2} \cos 6\varphi. \quad (21)$$

This energy correction has same symmetry, but the opposite sign compared to Eqs. (10) and (15). Hence, for $J_{\pm\pm} > 0$ the on-site disorder favors magnetic configurations (2) with $\varphi = \pi(1 + 2n)/6$. These correspond to six coplanar $m_{x^2-y^2}$ states.

B. Bond disorder

Another type of randomness in magnetic solids is bond disorder. In pyrochlore materials it may appear as a result of doping on the nonmagnetic B sites. We model this type of disorder by small random variations of J_\pm and $J_{\pm\pm}$:

$$\begin{aligned} J_\pm &\longrightarrow J_\pm^{ij} = J_\pm(1 + \delta_{ij}), \\ J_{\pm\pm} &\longrightarrow J_{\pm\pm}^{ij} = J_{\pm\pm}(1 + \delta_{ij}). \end{aligned} \quad (22)$$

The fluctuating part δ_{ij} is assumed to be uncorrelated between adjacent bonds and relatively small, $\langle \delta_{ij}^2 \rangle = D \ll 1$, such that it does not change the sign of exchange constants.

The subsequent calculation is completely similar to the previous subsection up to a substitution $\epsilon(p_i + p_j) \rightarrow \delta_{ij}$. The state-dependent energy correction has the form

$$\Delta E = -\frac{1}{(12J_\pm)^2} \sum_{\langle ij \rangle} M_{ij} K_{ij}^2 \delta_{ij}^2 \simeq \frac{J_{\pm\pm}^3 D N}{24J_\pm^2} \cos 6\varphi. \quad (23)$$

We conclude this section with the remark that a different state selection produced by structural disorder has its origin in the local breakdown of frustration. Indeed, the corresponding energy correction is determined by the linear term \hat{V}_1 , whereas thermal and quantum order from disorder stems from the quadratic part \hat{V}_2 . Technically, the two terms have different combinations of the relative angles as demonstrated by Eq. (6) for the XY pyrochlore antiferromagnet. In the Heisenberg case there is a similar change between \hat{V}_1 and \hat{V}_2 consisting in $\sin \theta_{ij}$ and $\cos \theta_{ij}$ prefactors, respectively, θ_{ij} being an angle between two spins [12]. Thus, we may claim that structural disorder has a *qualitatively* different effect on the ground-state selection in a frustrated magnet compared to thermal/quantum fluctuations. In the purely classical picture the structural disorder always wins over thermal fluctuations at low temperatures. In real frustrated magnets, the structural disorder must compete with quantum fluctuations for the state selection at $T = 0$. There is a critical strength of disorder or a critical impurity concentration above which the structural order from disorder effect prevails. More detailed consideration of these effects is postponed till Sec. VI.

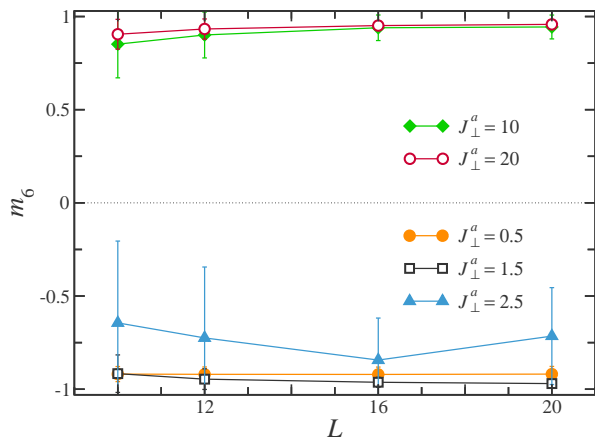


FIG. 2. (Color online) Zero-temperature results for the clock order parameter m_6 obtained for an XY pyrochlore antiferromagnet with $n_{\text{imp}} = 5\%$ of nonmagnetic impurities for several cluster sizes L and different values of the anisotropic exchange J_{\perp}^a . Positive and negative values of m_6 correspond to $m_{3z^2-r^2}$ and $m_{x^2-y^2}$ magnetic states, respectively.

V. NUMERICAL RESULTS

In this section we corroborate the analytic results obtained for weak disorder by numerical investigation of genuine vacancies in the classical anisotropic XY pyrochlore antiferromagnet. For that we return back to the original spin Hamiltonian (1) and set $J_{\perp} = 1$. Overall, we present two types of numerical data: determination of the ground-state magnetic structure at zero temperature and Monte Carlo simulations of finite-temperature properties. In both cases numerical computations were performed on periodic clusters of $N = 4L^3$ classical spins. Random vacancies were introduced by setting $|\mathbf{S}_i| = 0$ for a fixed number of sites $N_{\text{imp}} = n_{\text{imp}}N$. For all computations we employed about 100 independent impurity configurations used to average numerical data and to estimate the error bars.

For $J_{\perp}^a > 0$, magnetic states of the XY pyrochlore antiferromagnet are characterized by two order parameters:

$$m = \sqrt{m_x^2 + m_y^2}, \quad m_6 = \frac{1}{m^5} \text{Re}\{(m_x + im_y)^6\}. \quad (24)$$

Here, two components

$$m_x = \frac{1}{N} \sum_i \mathbf{S}_i \cdot \hat{\mathbf{x}}_i, \quad m_y = \frac{1}{N} \sum_i \mathbf{S}_i \cdot \hat{\mathbf{y}}_i \quad (25)$$

are defined using a specific choice of axes in the local xy planes, see Eq. (2). Basically, m discriminates ordering within the E -manifold from other irreducible representations of the tetrahedral group, whereas the clock parameter $m_6 = m \cos 6\varphi$ distinguishes between the different E -states [26]. The clock order parameter has a positive value for six noncoplanar states $m_{3z^2-r^2}$ and becomes negative for coplanar spin configurations $m_{x^2-y^2}$.

A. Ground state minimization

We begin with minimization of the classical energy (1) for a fixed concentration of static vacancies. We start with a random initial spin configuration and solve iteratively the classical energy minimum condition

$$\mathbf{S}_i = \mathbf{h}_i / |\mathbf{h}_i| \quad (26)$$

with \mathbf{h}_i being the local field on site i . After convergence is reached, the internal energy and the order parameters (24) are calculated. The process is repeated for 10^3 initial random spin configurations and the global minimum is chosen afterwards. Then, the whole procedure is repeated again for a new configuration of impurities. The final data are produced by averaging over the lowest energy magnetic structures obtained for each vacancy set.

Figure 2 shows our results for the clock order parameter m_6 in the XY pyrochlore antiferromagnet with $n_{\text{imp}} = 5\%$ of nonmagnetic impurities. For each value of the anisotropy parameter $J_{\perp}^a > 0$ we performed numerical minimization for several cluster-sizes up to $L = 20$. Negative values of m_6 confirm appearance of the coplanar $m_{x^2-y^2}$ state induced by impurities for $J_{\perp}^a < 4$. The absolute value of the order parameter grows with increasing cluster size leaving no doubts about the existence of the true long-range order. Likewise, for large $J_{\perp}^a > 4$ random impurities stabilize the noncoplanar $m_{3z^2-r^2}$ magnetic structure characterized by $m_6 > 0$.

The value $J_{\perp}^a = 4$ ($J_{\pm\pm} = 0$) corresponds to isotropic XY spin model in the site-dependent local frame. Consequently, two states, $m_{3z^2-r^2}$ and $m_{x^2-y^2}$, remain exactly degenerate for this value of J_{\perp}^a : neither thermal/quantum fluctuations [24] nor impurities (Sec. IV) can lift this degeneracy determined by an emergent $SO(2)$ rotational symmetry of the spin Hamiltonian. For J_{\perp}^a close to 4, convergence of the iterative procedure becomes very slow, see $L = 20$ point for $J_{\perp}^a = 2.5$ in Fig. 2. One needs to employ a significantly larger number of initial configurations to approach the true minimum state. This may indicate the development of some type of glassiness in the system. Similar effect is also present for very small $J_{\perp}^a \lesssim 0.1$ because of additional degeneracy appearing for $J_{\perp}^a = 0$, see Sec II. Finally, we studied numerical impurity concentrations in the range $0.5\% < n_{\text{imp}} < 7\%$ and obtained the ground state selection independent of n_{imp} .

B. Monte Carlo simulations

Monte Carlo simulations of the classical XY pyrochlore antiferromagnet were performed using the Metropolis algorithm alternating five Metropolis steps with five microcanonical over-relaxation sweeps [37] before every measurement. In total, $2 \cdot 10^5$ measurements were taken at every temperature and averaging was done over 100 impurity configurations. We simulated the

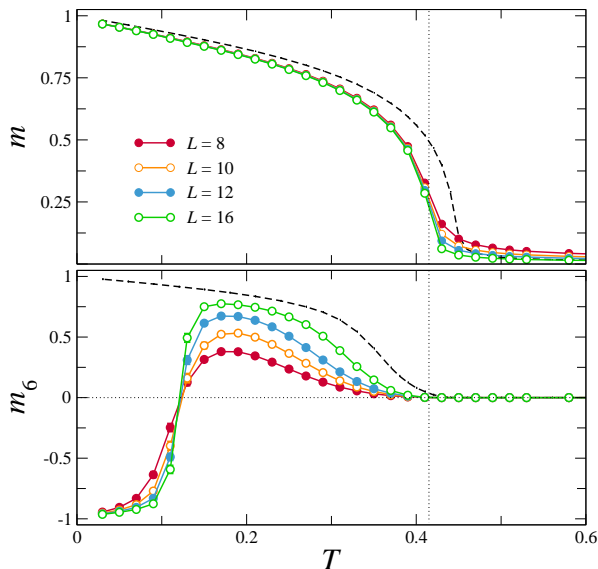


FIG. 3. (Color online) Monte Carlo results for the antiferromagnetic m (upper panel) and the clock m_6 (lower panel) order parameters for the XY pyrochlore antiferromagnet (1) with $J_{\perp}^a = 0.5$ and 5% of vacancies. Dotted vertical line indicates the transition temperature. Dashed lines show the behavior of m and m_6 for a pure system with $L = 16$.

model (1) restricting variation range of the anisotropy parameter to $0.3 \leq J_{\perp}^a \leq 2$.

Temperature dependence of the two order parameters m and m_6 for $J_{\perp}^a = 0.5$ and $n_{\text{imp}} = 5\%$ is shown in Fig. 3. The transition temperature $T_c = 0.415$ was determined from intersection of Binder cumulants $U_L = \langle m^4 \rangle / \langle m^2 \rangle^2$. It is somewhat reduced compared to the transition into the pure model $T_c^0 = 0.4454$ for the same value of J_{\perp}^a . The critical behavior of the model (1) belongs to the 3D XY universality class [26] with the known value of the correlation length exponent $\nu \approx 0.672$ [39]. We can now use the Harris criterion [38], which states that the critical behavior for phase transitions with $d\nu > 2$ remains unchanged in the presence of disorder. Since ν is slightly larger than $2/3$, the critical point in the XY pyrochlore antiferromagnet remains unaffected upon dilution with nonmagnetic impurities.

Nevertheless, the diluted antiferromagnet exhibits the peculiar temperature dependence of the clock order parameter m_6 , see the lower panel of Fig. 3. Right below T_c , m_6 is positive, as expected for the $m_{3z^2-r^2}$ state, and grows at fixed T with the system size L . Such ‘inverse’ finite-size scaling is attributed to the dangerously irrelevant role of the six-fold anisotropy at the XY transition in three dimensions and is explained by presence of an additional length-scale $\xi_6 \gg \xi$ [26]. Upon further cooling, the clock order parameter shows a sharp jump to negative values at $T_1 \approx 0.12$. This jump signifies a phase transition into the $m_{x^2-y^2}$ state stabilized by impurities. Basically, the temperature dependence of m_6 is determined by competition of two terms: the impurity

correction ΔE_2 given by Eq. (21) and the free-energy correction $\Delta F^{(3)}$ generated by thermal fluctuations (10). They have different sign and at $T \rightarrow 0$ the impurity contribution dominates selecting the $m_{x^2-y^2}$ state. However, thermal fluctuations grow with temperature and above T_1 the effective anisotropy $\Delta F^{(3)}$ wins over ΔE_2 leading to the $m_{3z^2-r^2}$ state right below T_c .

The phase transition between $m_{3z^2-r^2}$ and $m_{x^2-y^2}$ states is expected to be of the first order on symmetry grounds. (Another possibility is two closely located second-order transitions with an intermediate low-symmetry phase.) We collected histograms for the clock order parameter m_6 for a few impurity concentrations, which confirm the first-order nature of the transition. On the other hand, no anomaly is seen in the specific heat or magnetic susceptibility even for the largest clusters. A similar behavior was also observed in our previous study of the triangular Heisenberg antiferromagnet with vacancies [12]. Thermodynamic signatures of the first-order transition appear to be blurred by disorder.

The observed sequence of ordered phases remains stable under variations of n_{imp} and J_{\perp}^a . Figure 4 shows dependence on vacancy concentration for $J_{\perp}^a = 0.3$. We include only Monte Carlo results for the largest clusters with $L = 16$. The first-order transition temperature progressively grows between $T_1 = 0.025$ for $n_{\text{imp}} = 1\%$ to $T_1 = 0.125$ for $n_{\text{imp}} = 10\%$. The order parameter jump is very sharp for the lowest impurity concentration but becomes significantly smeared for $n_{\text{imp}} = 10\%$. We attribute this effect to a substantial finite-size scaling at large impurity concentrations. Monte Carlo simulations of significantly bigger clusters are required for precise determination of the transition point between the two E states for large density of vacancies.

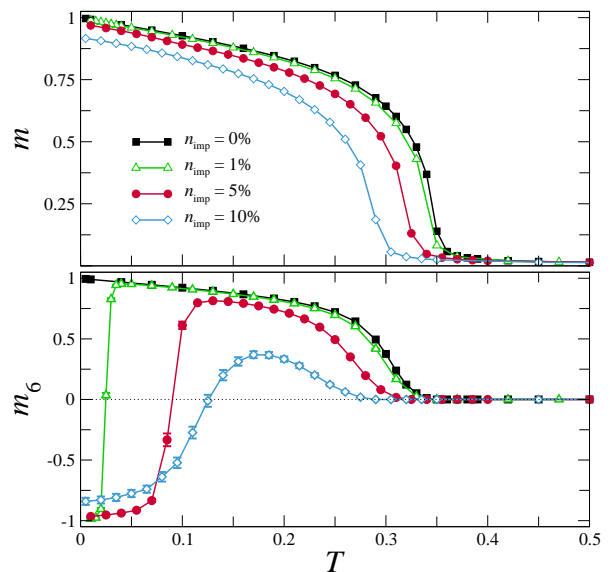


FIG. 4. (Color online) Temperature dependence of the magnetic order parameters for different impurity concentrations. Monte Carlo results are for $J_{\perp}^a = 0.3$ and $L = 16$.

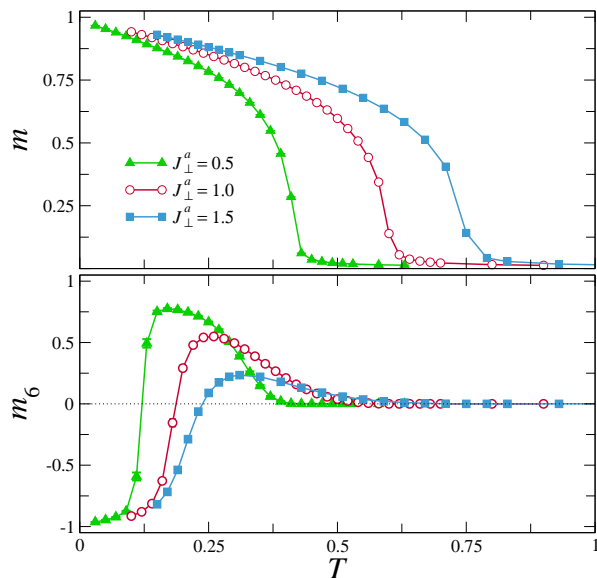


FIG. 5. (Color online) Temperature dependence of the magnetic order parameters for fixed impurity concentration $n_{\text{imp}} = 5\%$ and different values of J_{\perp}^a . Monte Carlo results are for $L = 16$ clusters.

Finally, dependence on J_{\perp}^a is illustrated in Fig. 5. As expected, the $m_{x^2-y^2}$ state is present at low temperatures for all studied values of the anisotropic exchange including $J_{\perp}^a = 1.5$, which is very close to the experimental estimate for $\text{Er}_2\text{Ti}_2\text{O}_7$, see Appendix A. Somewhat surprisingly, the thermal selection of the $m_{3z^2-r^2}$ state in the vicinity of T_c is also remarkably stable under variations of n_{imp} or J_{\perp}^a . This can be considered as a consequence of the Harris criterion, which asserts irrelevance of quenched disorder for transitions in the 3D XY universality class.

VI. STRUCTURAL VS QUANTUM DISORDER

The Monte Carlo results of the previous section give a general idea about competition between impurities and thermal fluctuations for the ground-state selection. Beyond the classical model, similar competition exists also for the structural disorder and quantum effects even at zero temperature. There must be a critical impurity concentration above which the quantum selection gives way to the spin configurations stabilized by vacancies. Since the energy gain produced by impurity substitution is a purely classical effect, the critical impurity concentration scales with the spin length as $n_c \sim 1/S$. This raises a legitimate question about observability of the structural order from disorder effect in spin-1/2 frustrated magnets, in particular, in diluted $\text{Er}_2\text{Ti}_2\text{O}_7$.

Even an approximate calculation of n_c is a fairly difficult theoretical problem. In order to treat quantum effects within the framework of the $1/S$ spin-wave expansion, one starts with setting up the Holstein-Primakoff

transformation from spins to bosons in the local frame around a specific magnetic state. Subsequent calculation of the quantum energy correction can be performed directly in the real space without a need to do the Fourier transformation [40 and 41]. Then, in full analogy with Sec. V A, one can find numerically the harmonic energy correction for an impurity-induced nonuniform spin texture and average that over random impurity configurations. However, a similar computation for the competing spin configurations selected by quantum fluctuations at $n_{\text{imp}} = 0$ immediately fails. Such states cease to be the classical ground states in the presence of impurities and, hence, have ill-defined harmonic excitation spectra. The quantum order by disorder selection is manifestly nonlinear effect in the presence of structural randomness.

Here, we circumvent the difficulty of treating nonlinear quantum effects for an impurity-induced spin texture in $\text{Er}_2\text{Ti}_2\text{O}_7$, by assuming that concentration of vacancies is low. Then, the quantum energy correction can be taken as that for the pure $S = 1/2$ pyrochlore antiferromagnet (15), whereas the classical energy gain from impurities is estimated from Eq. (21) by restoring the S^2 prefactor and substituting $\epsilon = 1$. Actually, instead of the harmonic result (15) we employ a more accurate expression (C7) with a 40% reduced amplitude for the sixfold harmonics due to renormalization by interaction effects. In this way we obtain a reasonably small value of the critical impurity concentration $n_c \approx 7\%$ being only weakly dependent on the ratio of $J_{\pm\pm}/J_{\pm}$. For comparison, the magnetization plateau in the Heisenberg triangular antiferromagnet remains stable up to $n_c \sim 20\%$ for $S = 1/2$ basically meaning that the dilution effects in this case are observable only for large spins $S \gtrsim 1$ [12].

Undoubtedly, the above estimate is rather crude and there are good chances that the critical impurity concentration for $\text{Er}_2\text{Ti}_2\text{O}_7$ is even smaller than 7%. The approximation adopted for derivation of (21) treats only tilting of nearest-neighbor spins around a vacancy. Inclusion of full-range spin relaxation in an impurity-induced magnetic texture should further increase the corresponding energy gain and, hence, reduce the critical value of n_{imp} . Thus, we may conclude that quantum effects become subdominant in the anisotropic XY pyrochlore already for small dilution and there is a good prospective for an experimental observation of the impurity induced $m_{x^2-y^2}$ state in $\text{Er}_2\text{Ti}_2\text{O}_7$.

VII. CONCLUSIONS

To summarize, we have studied the effect of nonmagnetic dilution and weak bond disorder for the anisotropic XY pyrochlore antiferromagnet. The degeneracy lifting produced by the two types of disorder is opposite to the effect of thermal and quantum fluctuations. Specifically, in the parameter range $J_{\perp}^a/J_{\perp} < 4$ relevant for $\text{Er}_2\text{Ti}_2\text{O}_7$, the structural disorder stabilizes at zero temperature the coplanar $m_{x^2-y^2}$ magnetic structure. At finite temper-

atures, thermal fluctuations induce the reentrant first-order transition into the $m_{3z^2-r^2}$ state. Our results further confirm the striking dissimilarity between the order from disorder effects generated by fluctuations, thermal or quantum, and by frozen disorder in the spin Hamiltonian parameters. In a broader prospective, the different ground-state selection is produced by different coupling to transverse spin fluctuations and, therefore, should persists for various generalizations of the spin Hamiltonian including frustrated spin-orbital models [42]. Finally, let us remark that completely unambiguous identification of the quantum order from disorder effect always meets a problem of distinguishing it from weak extra interactions like, for example, spin-lattice coupling in the case of the magnetization plateaus [43]. On the other hand, controlled doping of nonmagnetic impurities into a frustrated magnet may provide a clear experimental evidence of the structural order from disorder phenomenon.

ACKNOWLEDGMENTS

We are grateful to R. Moessner and M. Vojta for fruitful discussions.

Appendix A: Spin Hamiltonian

In cubic pyrochlore materials, magnetic ions form a network of corner-sharing tetrahedra usually called a pyrochlore lattice. The unit cell contains four magnetic sites. Their positions in units of the cubic lattice parameter a and the directions of local $\langle 111 \rangle$ axes are given by

$$\begin{aligned} \mathbf{r}_1 &= (0, 0, 0), & \hat{\mathbf{z}}_1 &= \frac{1}{\sqrt{3}}(1, 1, 1), \\ \mathbf{r}_2 &= (\frac{1}{4}, \frac{1}{4}, 0), & \hat{\mathbf{z}}_2 &= \frac{1}{\sqrt{3}}(-1, -1, 1), \\ \mathbf{r}_3 &= (0, \frac{1}{4}, \frac{1}{4}), & \hat{\mathbf{z}}_3 &= \frac{1}{\sqrt{3}}(1, -1, -1), \\ \mathbf{r}_4 &= (\frac{1}{4}, 0, \frac{1}{4}), & \hat{\mathbf{z}}_4 &= \frac{1}{\sqrt{3}}(-1, 1, -1). \end{aligned} \quad (\text{A1})$$

The primitive lattice vectors are chosen as $\mathbf{a}_1 = (\frac{1}{2}, \frac{1}{2}, 0)$, $\mathbf{a}_2 = (0, \frac{1}{2}, \frac{1}{2})$, and $\mathbf{a}_3 = (\frac{1}{2}, 0, \frac{1}{2})$.

The most general form of the anisotropic exchange Hamiltonian for pseudo-spin-1/2 operators representing erbium magnetic moments can be written as [7, 26]

$$\begin{aligned} \hat{\mathcal{H}} &= \sum_{\langle ij \rangle} J_{zz} S_i^z S_j^z + J_{\perp} \mathbf{S}_i^{\perp} \cdot \mathbf{S}_j^{\perp} + J_{\perp}^a (\mathbf{S}_i^{\perp} \cdot \hat{\mathbf{r}}_{ij}) (\mathbf{S}_j^{\perp} \cdot \hat{\mathbf{r}}_{ij}) \\ &+ J_{z\perp} [S_i^z (\mathbf{S}_i^{\perp} \cdot \hat{\mathbf{r}}_{ij}) + S_j^z (\mathbf{S}_j^{\perp} \cdot \hat{\mathbf{r}}_{ji})]. \end{aligned} \quad (\text{A2})$$

Here $\hat{\mathbf{r}}_{ij} = (\mathbf{r}_i - \mathbf{r}_j)/|\mathbf{r}_i - \mathbf{r}_j|$ is a unit vector in the bond direction. Spin operators \mathbf{S}_i are taken in the local coordinate frame with S_i^z and \mathbf{S}^{\perp} being projections on the local trigonal axis and on the orthogonal xy plane, respectively. Being independent of the choice of x and y

axes, this form of the Hamiltonian is convenient for calculation of classical energies and for Monte Carlo simulations.

To describe the classical ground states of the XY pyrochlore antiferromagnet we choose directions of $\hat{\mathbf{x}}_i$ and $\hat{\mathbf{y}}_i$ axes such that they coincide with sublattice direction for the $m_{3z^2-r^2}$ and the $m_{x^2-y^2}$ state, respectively:

$$\begin{aligned} \hat{\mathbf{x}}_1 &= \frac{1}{\sqrt{6}}(1, 1, -2), & \hat{\mathbf{y}}_1 &= \frac{1}{\sqrt{2}}(-1, 1, 0), \\ \hat{\mathbf{x}}_2 &= \frac{1}{\sqrt{6}}(-1, -1, -2), & \hat{\mathbf{y}}_2 &= \frac{1}{\sqrt{2}}(1, -1, 0), \\ \hat{\mathbf{x}}_3 &= \frac{1}{\sqrt{6}}(1, -1, 2), & \hat{\mathbf{y}}_3 &= \frac{1}{\sqrt{2}}(-1, -1, 0), \\ \hat{\mathbf{x}}_4 &= \frac{1}{\sqrt{6}}(-1, 1, 2), & \hat{\mathbf{y}}_4 &= \frac{1}{\sqrt{2}}(1, 1, 0). \end{aligned} \quad (\text{A3})$$

The spin Hamiltonian used in Sec. III is derived from an alternative form of the spin Hamiltonian (A2):

$$\begin{aligned} \hat{\mathcal{H}} &= \sum_{\langle ij \rangle} \left\{ J_{zz} S_i^z S_j^z - J_{\pm} (S_i^+ S_j^- + S_i^- S_j^+) \right. \\ &+ J_{\pm\pm} (e^{i\gamma_{ij}} S_i^+ S_j^+ + e^{-i\gamma_{ij}} S_i^- S_j^-) \\ &\left. - J_{z\pm} [S_j^z (e^{-i\gamma_{ij}} S_i^+ + e^{i\gamma_{ij}} S_i^-) + i \leftrightarrow j] \right\}, \end{aligned} \quad (\text{A4})$$

were phases γ_{ij} explicitly depend on the choice of basis in the xy planes. This form of the spin Hamiltonian was previously employed in a number of works [8, 44, 45] with a minor redefinition of complex factors. Instead of using $\gamma_{ij} \equiv e^{i\gamma_{ij}}$ and $\zeta_{ij} \equiv -e^{-i\gamma_{ij}}$, we explicitly extract phases, which greatly simplifies our subsequent expressions. For the above choice of axes we have

$$\gamma_{12} = \gamma_{34} = 0, \quad \gamma_{13} = \gamma_{24} = -\gamma_{14} = -\gamma_{23} = \frac{2\pi}{3}. \quad (\text{A5})$$

Comparing two forms of the spin Hamiltonian we obtain the following relation between two sets of exchange parameters:

$$\begin{aligned} J_{\perp} &= 2(J_{\pm} + J_{\pm\pm}), & J_{\perp}^a &= 8J_{\pm} - 4J_{\pm\pm}, \\ J_{z\perp} &= -2\sqrt{3}J_{z\pm}. \end{aligned} \quad (\text{A6})$$

Neutron measurements of magnetic excitations in $\text{Er}_2\text{Ti}_2\text{O}_7$ in a high magnetic field [8], yield the following estimate for the exchange parameters in 10^{-2} meV:

$$\begin{aligned} J_{\pm} &= 6.5 \pm 0.75, & J_{\pm\pm} &= 4.2 \pm 0.5, \\ J_{zz} &= -2.5 \pm 1.8, & J_{z\pm} &= -0.88 \pm 1.5. \end{aligned} \quad (\text{A7})$$

Applying (A6) we obtain

$$\begin{aligned} J_{\perp} &= 0.21(2) \text{ meV}, & J_{\perp}^a &= 0.35(5) \text{ meV}, \\ J_{zz} &= -0.025(2) \text{ meV}, & J_{z\perp} &= 0.03(5) \text{ meV}. \end{aligned} \quad (\text{A8})$$

The above values confirm the planar character of the interaction between Er^{3+} moments as well as a significant anisotropy for the in-plane exchange constants $J_{\perp}^a/J_{\perp} \approx 1.7$. Since transverse exchange constants J_{zz} and $J_{z\perp}$ are an order of magnitude smaller, the physical properties $\text{Er}_2\text{Ti}_2\text{O}_7$ can be quite accurately captured by the model with just two exchange parameters J_{\perp} and J_{\perp}^a or J_{\pm} and $J_{\pm\pm}$ used in the main text.

Appendix B: Quantum order by disorder

Here we provide more details on the calculation of the quantum correction (15), which selects between different classical spin configurations. The basic set up of the perturbation expansion is described in Sec. III, see Eqs. (6) and (7). The ground state $|0\rangle$ of the noninteracting Hamiltonian \hat{H}_0 coincides with a classical state and corresponds to a fully-saturated state in the local basis: $S_i^+|0\rangle = 0$. As a result, the perturbation series starts with the second-order correction

$$\Delta E^{(2)} = \sum_n \frac{\langle 0|\hat{V}|n\rangle\langle n|\hat{V}|0\rangle}{E_0 - E_n}. \quad (\text{B1})$$

Due to the specific form of the perturbation $\hat{V} = V_2 + V_3$, the intermediate excited states $|n\rangle$ have only two spin flips on neighboring lattice sites with $E_n = E_0 + 2h$. These processes are represented by the following diagram:

$$|00\rangle \xrightarrow{S_i^- S_j^-} |11\rangle \xrightarrow{S_i^+ S_j^+} |00\rangle, \quad (\text{B2})$$

which describes creation and subsequent annihilation of a pair of spin flips on the same bond $\langle ij\rangle$. The energy correction from these processes is

$$\Delta E^{(2)} = - \sum_{\langle ij\rangle} \frac{S^2}{4} \frac{M_{ij}^2}{2h} = - \frac{NSJ_{\pm}}{8} \left(1 + \frac{J_{\pm\pm}^2}{2J_{\pm}^2}\right). \quad (\text{B3})$$

Absence of φ -dependence in the final expression can be easily understood by noticing that $M_{ij} \propto \cos 2\varphi$ and, consequently, $\Delta E^{(2)} \propto \cos 4\varphi$. However, all lower-order φ -harmonics are prohibited by the Z_6 symmetry with the proper angular-dependent contribution $\Delta E \sim M_{ij}^3 \propto \cos 6\varphi$ arising only in the third order of the perturbation expansion.

The third-order energy correction is given by the Rayleigh-Schrödinger expression (12). In this order, there are two distinct excitation processes. The first one considered in the main text is represented by the triangular plaquette diagram

$$|000\rangle \xrightarrow{S_i^- S_j^-} |110\rangle \xrightarrow{S_j^+ S_k^-} |101\rangle \xrightarrow{S_k^+ S_i^+} |000\rangle. \quad (\text{B4})$$

The full expression of the corresponding energy correction is given by (14) and after summation transforms into

$$\Delta E^{(3a)} = - \frac{J_{\pm\pm}^3 NS}{192 J_{\pm}^2} \cos 6\varphi - \frac{NSJ_{\pm}}{48} \left(1 - \frac{3J_{\pm\pm}^2}{4J_{\pm}^2}\right). \quad (\text{B5})$$

The scaling $\Delta E^{(3a)} \sim JS$ indicates that this correction is one of the terms included into the harmonic spin-wave theory. Thus, we may directly compare the analytic expression (B5) to the full ground-state energy correction of the harmonic spin-wave theory, which requires numerical integration of magnon energies over the Brillouin zone. Results are presented in Fig. 6. The inset shows $\Delta E_{\text{g.s.}}$

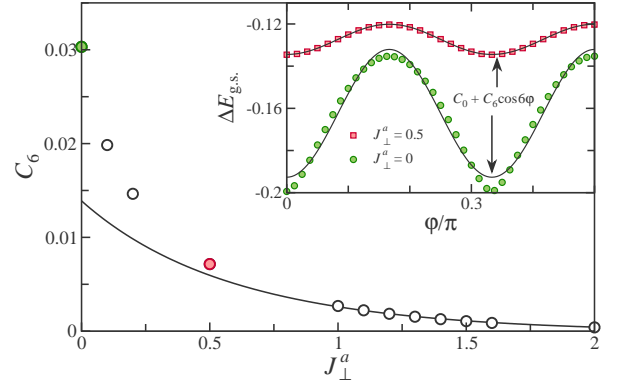


FIG. 6. (Color online) Inset: fit of the spin-wave energy correction $\Delta E_{\text{g.s.}}$ (data points) to $\cos 6\varphi$ angular dependence (full lines). Main panel: comparison of the fitted amplitude C_6 of the cosine function (circles) to the analytic expression (solid line) from the leading term in the harmonic expansion (B5).

for $J_{\perp}^a/J_{\perp} = 0$ and 0.5 (data points) from Ref. 7 and fits to

$$\Delta E_{\text{g.s.}} = C_0 + C_6 \cos 6\varphi \quad (\text{B6})$$

dependence (full lines). The $J_{\perp}^a/J_{\perp} = 0$ data exhibit the required sixfold periodicity but noticeably deviate from a simple cosine function. On the other hand, for $J_{\perp}^a/J_{\perp} = 0.5$ and larger, the spin-wave data are perfectly fitted by Eq. (B6). Values of C_6 obtained from the fit are compared to the analytic expression (B5) in the main panel of Fig. 6. The agreement is very good for $J_{\perp}^a/J_{\perp} \gtrsim 1$ signaling that accuracy of the analytic result is basically governed by a small ratio

$$\frac{J_{\pm\pm}}{J_{\pm}} = \frac{4J_{\perp} - J_{\perp}^a}{2J_{\perp} + J_{\perp}^a}. \quad (\text{B7})$$

We have also compared the constant C_0 to φ -independent contributions in Eqs. (B3) and (B5) and found agreement within 15–25%, which is a reasonable accuracy for just two first terms of the $1/z$ expansion.

Another third-order contribution is described by the diagram

$$|00\rangle \xrightarrow{S_i^- S_j^-} |11\rangle \xrightarrow{S_i^+ S_j^+} |11\rangle \xrightarrow{S_i^+ S_j^+} |00\rangle \quad (\text{B8})$$

and corresponds to a single-bond process providing correction to (B3) due to interaction of two spin flips generated by \hat{V}_3 . Its explicit expression is

$$\Delta E^{(3b)} = \sum_{\langle ij\rangle} \frac{S^2}{4} \frac{M_{ij}^2 h_{ij}}{(24J_{\pm} S)^2}. \quad (\text{B9})$$

This energy correction also has a φ -dependent part:

$$\Delta E^{(3b)} \simeq \frac{NJ_{\pm\pm}^3}{384J_{\pm}^2} \cos 6\varphi. \quad (\text{B10})$$

The coefficient in front of the cosine function is positive providing an opposite tendency compared to $\Delta E^{(3a)}$. Still, for $S \geq 1$ and $J_{\pm\pm} > 0$ the total third-order correction robustly selects the $m_{3z^2-r^2}$ states. However, for the case $S = 1/2$ relevant to $\text{Er}_2\text{Ti}_2\text{O}_7$, the two angular-dependent terms cancel each other and one needs to perform a more careful analysis of the real-space perturbation terms. We present further details on that in the next Appendix, though the main conclusion on the state selection by quantum fluctuations remains intact.

Appendix C: Quantum perturbation theory for $S = 1/2$

In Appendix B we have found that the third-order quantum correction $\Delta E^{(3b)}$ resulting from interaction of two spin flips cancels the harmonic spin-wave contribution $\Delta E^{(3a)}$ leaving intact the degeneracy between $m_{3z^2-r^2}$ and $m_{x^2-y^2}$ states. To treat more carefully interaction effects we adopt a modified real-space expansion based on a partial rearrangement of perturbation terms in Eq. (7). Specifically, \hat{V}_3 is now included into a new unperturbed Hamiltonian

$$\hat{\mathcal{H}}'_0 = h \sum_i (S - S_i^z) + \sum_{\langle ij \rangle} h_{ij} (S - S_i^z)(S - S_j^z). \quad (\text{C1})$$

In this way the Ising part of spin-flip interaction is treated exactly. Basically, the new expansion corresponds to re-summation of an infinite subset of terms in the original real-space approach used in Sec. III and Appendix B. A similar trick was also applied in Ref. 31 for the Ising expansion at the fractional magnetization plateaus.

The main difference between the two forms of the real-space expansion is in assignment of excitation energies in (B1). The lowest-energy excitation, a pair of spin-flips on the same bond, costs now $E_n - E_0 = 2h + h_{ij}$. We

rewrite it as

$$E_n - E_0 = 2J_{\pm}\varepsilon + 2J_{\pm\pm} \cos(2\varphi + \gamma_{ij}), \quad (\text{C2})$$

with $\varepsilon = (12S - 1)$ and use $1/\varepsilon$ as a small parameter.

The second-order energy correction corresponds to single-bond processes and is expressed by

$$\Delta E^{(2)} = -\frac{S^2}{4} \sum_{\langle ij \rangle} \frac{M_{ij}^2}{2h + h_{ij}}. \quad (\text{C3})$$

Keeping only the lowest-order terms up to $O(\varepsilon^{-3})$ and dropping all unessential constants we obtain

$$\Delta E^{(2)} \simeq \frac{3NS^2J_{\pm\pm}^3}{8J_{\pm}^2\varepsilon^3}(\varepsilon - 2) \cos 6\varphi. \quad (\text{C4})$$

For large S this expression matches exactly with the corresponding term in $\Delta E^{(3b)}$, see (B10).

In the third-order, there is only a triangular-plaquette process, which provides the energy shift

$$\Delta E^{(3)} = -6 \sum_{\Delta} \frac{S^3}{8} \frac{M_{ij}M_{ki}M_{kj}}{(2h + h_{ij})(2h + h_{ik})}. \quad (\text{C5})$$

We calculate it expanding in powers of $1/\varepsilon$ as

$$\Delta E^{(3)} \simeq -\frac{N}{16} \frac{S^2J_{\pm\pm}^3}{J_{\pm}^2\varepsilon^3} \left(\varepsilon^2 + \varepsilon + \frac{3}{4} \frac{J_{\pm\pm}^2}{J_{\pm}^2} \right) \cos 6\varphi. \quad (\text{C6})$$

The first leading term again matches the angular-dependent part of the previous expression (B5).

Comparing now $\Delta E^{(2)}$ and $\Delta E^{(3)}$, we do see cancellation of the leading $1/\varepsilon$ terms for $S = 1/2$. Still the coefficient in front of the cosine is negative:

$$\Delta E = -\frac{3}{2000} \frac{NJ_{\pm\pm}^3}{J_{\pm}^2} \left(1 + \frac{1}{16} \frac{J_{\pm\pm}^2}{J_{\pm}^2} \right) \cos 6\varphi. \quad (\text{C7})$$

Thus, for $S = 1/2$ the quantum order by disorder selection acts in the same way as for large spins. The main consequence of spin flip interactions is $\sim 40\%$ reduction of the amplitude of the cosine harmonics as compared to the noninteracting result (15) or (B5).

¹ J. Villain, R. Bidaux, J.-P. Carton, and R. Conte, *J. de Physique* **41**, 1263 (1980).
² E. F. Shender, *Zh. Eksp. Teor. Fiz.* **83**, 326 (1982) [*Sov. Phys. JETP* **56**, 178 (1982)].
³ T. Inami, Y. Ajiro, and T. Goto, *J. Phys. Soc. Jpn.* **65**, 2374 (1996).
⁴ A. I. Smirnov, H. Yashiro, S. Kimura, M. Hagiwara, Y. Narumi, K. Kindo, A. Kikkawa, K. Katsumata, A. Ya. Shapiro, and L. N. Demianets, *Phys. Rev. B* **75**, 134412 (2007).
⁵ N. A. Fortune, S. T. Hannahs, Y. Yoshida, T. E. Sherline,

T. Ono, H. Tanaka, and Y. Takano, *Phys. Rev. Lett.* **102**, 257201 (2009).
⁶ T. Susuki, N. Kurita, T. Tanaka, H. Nojiri, A. Matsuo, K. Kindo, and H. Tanaka, *Phys. Rev. Lett.* **110**, 267201 (2013).
⁷ M. E. Zhitomirsky, M. V. Gvozdikova, P. C. W. Holdsworth, and R. Moessner, *Phys. Rev. Lett.* **109**, 077204 (2012).
⁸ L. Savary, K. A. Ross, B. D. Gaulin, J. P. C. Ruff, and L. Balents, *Phys. Rev. Lett.* **109**, 167201 (2012).
⁹ C. L. Henley, *Phys. Rev. Lett.* **62**, 2056 (1989).
¹⁰ Y. V. Fyodorov and E. F. Shender, *J. Phys.: Condens.*

- Matter **3**, 9123 (1991).
- ¹¹ C. Weber and F. Mila, Phys. Rev. B **86**, 184432 (2012).
 - ¹² V. S. Maryasin and M. E. Zhitomirsky, Phys. Rev. Lett. **111**, 247201, (2013).
 - ¹³ M. T. Heinilä and A. S. Oja, Phys. Rev. B **48**, 7227 (1993).
 - ¹⁴ B. Canals and M. E. Zhitomirsky, J. Phys.: Condens. Matter **16**, S759 (2004).
 - ¹⁵ J. C. Slonczewski, Phys. Rev. Lett. **67**, 3172 (1991).
 - ¹⁶ J. D. M. Champion, M. J. Harris, P. C. W. Holdsworth, A. S. Wills, G. Balakrishnan, S. T. Bramwell, E. Čížmár, T. Fennell, J. S. Gardner, J. Lago, D. F. McMorro, M. Orendáč, A. Orendáčová, D. McK. Paul, R. I. Smith, M. T. F. Telling, and A. Wildes, Phys. Rev. B **68**, 020401(R) (2003).
 - ¹⁷ A. Poole, A. S. Wills, and E. Lelièvre-Berna, J. Phys.: Condens. Matter **19**, 452201 (2007).
 - ¹⁸ J. P. C. Ruff, J. P. Clancy, A. Bourque, M. A. White, M. Ramazanoglu, J. S. Gardner, Y. Qiu, J. R. D. Copley, M. B. Johnson, H. A. Dabkowska, and B. D. Gaulin, Phys. Rev. Lett. **101**, 147205 (2008).
 - ¹⁹ S. S. Sosin, L. A. Prozorova, M. R. Lees, G. Balakrishnan, and O. A. Petrenko, Phys. Rev. B **82**, 094428 (2010).
 - ²⁰ P. Dalmas de Réotier, A. Yaouanc, Y. Chapuis, S. H. Curnoe, B. Grenier, E. Ressouche, C. Marin, J. Lago, C. Baines, and S. R. Giblin, Phys. Rev. B **86**, 104424 (2012).
 - ²¹ P. Bonville, S. Petit, I. Mirebeau, J. Robert, E. Lhotel, and C. Paulsen, J. Phys.: Condens. Matter **25**, 275601 (2013).
 - ²² K. A. Ross, Y. Qiu, J. R. D. Copley, H. A. Dabkowska, and B. D. Gaulin, Phys. Rev. Lett. **112**, 057201 (2014).
 - ²³ J. D. M. Champion and P. C. W. Holdsworth, J. Phys.: Condens. Matter **16**, S665 (2004).
 - ²⁴ A. W. C. Wong, Z. Hao, and M. J. P. Gingras, Phys. Rev. B **88**, 144402 (2013).
 - ²⁵ P. A. McClarty, P. Stasiak, and M. J. P. Gingras, Phys. Rev. B **89**, 024425 (2014).
 - ²⁶ M. E. Zhitomirsky, P. C. W. Holdsworth, and R. Moessner, Phys. Rev. B **89**, 140403(R) (2014).
 - ²⁷ X. Ke, R. S. Freitas, B. G. Ueland, G. C. Lau, M. L. Dahlberg, R. J. Cava, R. Moessner, and P. Schiffer, Phys. Rev. Lett. **99**, 137203 (2007).
 - ²⁸ L. J. Chang, Y. Su, Y.-J. Kao, Y. Z. Chou, R. Mittal, H. Schneider, Th. Brückel, G. Balakrishnan, and M. R. Lees, Phys. Rev. B **82**, 172403 (2010).
 - ²⁹ S. E. Palmer and J. T. Chalker, Phys. Rev. B **62**, 488 (2000).
 - ³⁰ M. W. Long, J. Phys.: Condens. Matter **1**, 2857 (1989).
 - ³¹ D. L. Bergman, R. Shindou, G. A. Fiete, and L. Balents, J. Phys.: Condens. Matter **19** 145204 (2007).
 - ³² K. H. Höglund, A. W. Sandvik, and S. Sachdev, Phys. Rev. Lett. **98**, 087203 (2007).
 - ³³ S. Eggert, O. F. Syljuåsen, F. Anfuso, and M. Andres, Phys. Rev. Lett. **99**, 097204 (2007).
 - ³⁴ A. Wollny, L. Fritz, and M. Vojta, Phys. Rev. Lett. **107**, 137204 (2011).
 - ³⁵ A. Sen, K. Damle, and R. Moessner, Phys. Rev. Lett. **106**, 127203 (2011).
 - ³⁶ A. Wollny, E. C. Andrade, and M. Vojta, Phys. Rev. Lett. **109**, 177203 (2012).
 - ³⁷ M. Creutz, Phys. Rev. D **36**, 515 (1987).
 - ³⁸ A. B. Harris, J. Phys. C **7**, 1671 (1974).
 - ³⁹ M. Campostrini, M. Hasenbusch, A. Pelissetto, and E. Vicari, Phys. Rev. B **74**, 144506 (2006).
 - ⁴⁰ S. Wessel and I. Milat, Phys. Rev. B **71**, 104427 (2005).
 - ⁴¹ O. Tchernyshyov, H. Yao, and R. Moessner, Phys. Rev. B **69**, 212402 (2004).
 - ⁴² G. Khaliullin, Prog. Theor. Phys. Suppl. **160**, 155 (2005).
 - ⁴³ K. Penc, N. Shannon, and H. Shiba, Phys. Rev. Lett. **93**, 197203 (2004).
 - ⁴⁴ S. Onoda and Y. Tanaka, Phys. Rev. Lett. **105**, 047201 (2010).
 - ⁴⁵ K. A. Ross, L. Savary, B. D. Gaulin, and L. Balents, Phys. Rev. X **1**, 021002 (2011).